Serial femtosecond X-ray diffraction of enveloped virus microcrystals

Robert M. Lawrence,[1,2,3] Chelsie E. Conrad,[1,3,4] Nadia A. Zatsepin,[1,3,5] Thomas D. Grant,[6,7] Haiguang Liu,[5,8] Daniel James,[1,3,5] Garrett Nelson,[1,3,5] Ganesh Subramanian,[1,3,5] Andrew Aquila,[9] Mark S. Hunter,[9] Mengning Liang,[9] Sébastien Boutet,[9] Jesse Coe,[1,3,4] John C. H. Spence,[1,3,5] Uwe Weierstall,[1,3,5] Wei Liu,[1,3,4] Petra Fromme,[1,3,4] Vadim Cherezov,[10] and Brenda G. Hogue[1,2,3,11,a)]

[1]*Biodesign Institute, Arizona State University, Tempe, Arizona 85287, USA*
[2]*Center for Infectious Diseases and Vaccinology, Arizona State University, Tempe, Arizona 85287, USA*
[3]*Center for Applied Structural Discovery, Arizona State University, Tempe, Arizona 85287, USA*
[4]*Department of Chemistry and Biochemistry, Arizona State University, Tempe, Arizona 85287, USA*
[5]*Department of Physics, Arizona State University, Tempe, Arizona 85287, USA*
[6]*Hauptman-Woodward Institute, State University of New York, Buffalo, New York 14203, USA*
[7]*Department of Structural Biology, State University of New York, Buffalo, New York 14203, USA*
[8]*Beijing Computational Science Research Center, Beijing 100084, China*
[9]*Linac Coherent Light Source, SLAC National Accelerator Laboratory, Menlo Park, California 94025, USA*
[10]*Department of Chemistry, Bridge Institute, University of Southern California, Los Angeles, California 90089, USA*
[11]*School of Life Sciences, Arizona State University, Tempe, Arizona 85287, USA*

(Received 12 March 2015; accepted 12 August 2015; published online 20 August 2015)

Serial femtosecond crystallography (SFX) using X-ray free-electron lasers has produced high-resolution, room temperature, time-resolved protein structures. We report preliminary SFX of Sindbis virus, an enveloped icosahedral RNA virus with ~700 Å diameter. Microcrystals delivered in viscous agarose medium diffracted to ~40 Å resolution. Small-angle diffuse X-ray scattering overlaid Bragg peaks and analysis suggests this results from molecular transforms of individual particles. Viral proteins undergo structural changes during entry and infection, which could, in principle, be studied with SFX. This is an important step toward determining room temperature structures from virus microcrystals that may enable time-resolved studies of enveloped viruses. [http://dx.doi.org/10.1063/1.4929410]

I. INTRODUCTION

A broadly distinguishing structural feature of all viruses is the presence or absence of a lipid envelope. Non-enveloped viruses are composed of structural proteins arranged in the form of a shell (capsid) that encloses a genome of either DNA or RNA. Enveloped viruses have, in addition, a lipid membrane that is acquired from host cells. The genomes of enveloped viruses are enclosed in a protein capsid or associated with protein as a helical nucleocapsid. Viral

a)Author to whom correspondence should be addressed. Electronic mail: Brenda.Hogue@asu.edu

glycoproteins are anchored in the lipid envelope. While some enveloped viruses are pleomorphic, others have a defined structure with symmetry and a fixed number of envelope proteins. Examples of human viruses that are enveloped and also possess structural symmetry include herpes simplex, varicella zoster, Epstein-Barr (*Herpesviridae*); dengue, West Nile, Yellow Fever (*Flaviviridae*); and Chikungunya (*Togaviridae*) viruses (Carstens, 2012).

A. Virus crystallography

Numerous X-ray crystallography structures have been determined from crystals of non-enveloped viruses, with resolution now reaching to 1.4 Å (Zocher *et al.*, 2014). Enveloped virus crystals, on the other hand, have not yet proven capable of producing such high-resolution diffraction. Although they are not typical enveloped viruses, X-ray structures from the lipid membrane-containing PRD1 (*Tectiviridae*) and PM2 (*Corticoviridae*) bacteriophage capsids have been reported to 4.2 Å (PDB ID: 1W8X) and 7.0 Å (PDB ID: 2W0C), respectively (Abrescia *et al.*, 2004; 2008). To date, no X-ray structure has been determined for a typical enveloped virus, which has a lipid membrane with envelope proteins that surrounds an inner capsid or nucleocapsid. Many such enveloped viruses are pleomorphic and lack the structural symmetry required for crystallization. Among the enveloped viruses that do possess a symmetrical physical structure, only Sindbis virus (*Togaviridae*), Semliki Forest virus (*Togaviridae*), and West Nile virus (*Flaviviridae*) have been crystallized (Wiley and von Bonsdorff, 1978; Harrison *et al.*, 1992; and Kaufmann *et al.*, 2010). X-ray diffraction was previously reported for Sindbis crystals at 30 Å (Harrison *et al.*, 1992), and West Nile virus crystals at 25 Å (Kaufmann *et al.*, 2010). Although enveloped viruses such as these possess a fixed number of proteins arranged with icosahedral symmetry in the envelope, high-resolution diffraction data remain elusive. It has been suggested that resolution is limited because the envelope lipids confer an inherent flexibility and heterogeneity to the virus particles (Rossmann, 2013). The motivation to crystallize other enveloped viruses has decreased as cryo-electron microscopy (cryo-EM) techniques have advanced significantly in recent years, leading to higher resolution image reconstructions of enveloped viruses (Grigorieff and Harrison, 2011). Cryo-EM maps have been obtained for Sindbis virus at 7 Å and 10.3 Å for West Nile virus (PDB: 3J0F, 3J0B) (Tang *et al.*, 2011 and Zhang *et al.*, 2013b). The highest resolution obtained for an enveloped virus with cryo-EM methods is currently the 3.5 Å map for dengue virus (*Flaviviridae*) (Zhang *et al.*, 2013a). The current application of cryo-EM for high-resolution structural studies is outstanding. The development and exploration of serial femtosecond crystallography (SFX) for virus studies are complementary to cryo-EM, as it allows for analysis of virus crystals at room temperature and has the potential to capture changes that viral proteins undergo during infection by time-resolved SFX experiments in the future.

Virus particles are several orders of magnitude larger in size and mass than proteins. Consequently, virus crystals often have significantly larger unit cells that typically contain only one or two viruses. The reduced number of unit cells per volume, compared to the same volume of smaller unit cells (smaller macromolecules), results in proportionally weaker X-ray diffraction. Diffraction patterns of crystals with large unit cells feature very densely spaced Bragg reflections and therefore, a larger number of reflections at a given resolution shell (Fry *et al.*, 1999; Rossmann, 1999; and Holton and Frankel, 2010). The dense spacing of the Bragg spots demands a large array of detector pixels to provide adequate sampling of the reflection and the areas between spots at high resolution. Thus, increases in the brilliance of X-ray sources and sensitivity of detectors are particularly beneficial for the study of virus crystals.

B. X-ray free-electron laser (XFEL) with viruses

The new method of SFX with XFEL (Chapman *et al.*, 2011 and Weierstall, 2014) represents a powerful advancement in the field of X-ray crystallography. Damage free crystal structures can now be determined from nano- and microcrystals of proteins that are difficult to crystallize and highly important, such as human G-protein coupled receptors (GPCRs) (Liu *et al.*, 2013; Fenalti *et al.*, 2015; and Zhang *et al.*, 2015). The technique is beginning to

have a significant impact in biology and medicine. The unparalleled brilliance of XFEL beams and short femtosecond pulse duration that outruns radiation damage (Barty *et al.*, 2011) makes them uniquely well-suited for studying viruses as crystals and as single particles. Thus far, only low resolution XFEL diffraction has been reported from large viruses that were probed as single particles (Song *et al.*, 2008; Seibert *et al.*, 2011; and Ekeberg *et al.*, 2015). Here, we present the first diffraction results from SFX studies of enveloped virus crystals.

XFELs allow the collection of data prior to onset of radiation damage at room temperature, rather than under cryo-conditions (Barty *et al.*, 2011 and Chapman *et al.*, 2014). This enables for the first time damage-free collection of X-ray diffraction data from biological samples under physiological conditions. Furthermore, the physiological conditions can be dynamically controlled during delivery of sample to the XFEL beam to produce time-resolved diffraction data (Aquila *et al.*, 2012; Kupitz *et al.*, 2014; Spence, 2014; Tenboer *et al.*, 2014; and Wang *et al.*, 2014). Recently, it has been shown that structural changes can be detected by time-resolved SFX at atomic resolution (Tenboer *et al.*, 2014). Many viruses undergo structural changes during their life cycles, including response to changes in pH during entry via endosomes and viral protein interactions with cellular receptors (Perera *et al.*, 2008; Connolly *et al.*, 2011; and Harrison *et al.*, 2013). The application of time-resolved SFX to understand these changes has significant potential for structural virology studies. Recently, it has been shown that detailed time-resolved structural changes can be detected by wide angle X-ray scattering of single proteins in solution using an XFEL when there is a corresponding initial-state structure available at high resolution that can be used as a reference point (Neutze, 2014). The high-resolution static virus structures that are now becoming attainable with cryo-EM can potentially be combined with dynamic room-temperature studies of conformational changes studied with time-resolved SFX in a powerful complementary approach toward producing time-resolved virus structures.

C. Sindbis as a structural model for enveloped virus crystals

Sindbis virus is a member of the *Togaviridae* family, which also includes other medically important viruses such as Chikungunya virus, Ross River virus, Semliki Forest virus, and Rubella virus. All viruses included in the *Togaviridae* are enveloped, positive-sense, and single-stranded RNA viruses. Sindbis is transmitted from mosquitoes to humans and other vertebrates (Lundstrom and Pfeffer, 2010). It has been used as a structural model for the study of enveloped viruses in past decades because it grows to high titers and exhibits icosahedral symmetry in both its capsid and envelope (Zhang *et al.*, 2002 and Hernandez and Brown, 2005). Small angle neutron scattering (SANS) measurements determined the diameter of Sindbis as 676 ± 25 Å at pH 7.2 and 720 ± 28 Å at pH 6.4 (He *et al.*, 2012). Sindbis is composed of three major structural components, two envelope glycoproteins (E1 and E2) and one capsid protein (C). There are 240 copies of each of these proteins per virus particle. In the envelope, E1 and E2 form heterodimers that further associate as trimers. The $T = 4$ icosahedral symmetry of Sindbis is defined by the 80 resulting E1-E2 trimeric spikes that are anchored in the lipid envelope. Inside the envelope, the 240 capsid proteins are also organized into an icosahedron with $T = 4$ symmetry. The ~11.7 kb RNA genome is packaged inside the capsid. Protein, RNA, and lipids constitute roughly 64%, 9%, and 27%, respectively, of the total viral mass of Sindbis virus particles (Fuller, 1987).

The ability to grow a large amount of Sindbis virus, its icosahedral symmetry, and availability of structural details from cryo-EM make crystals of the virus an ideal model for development of SFX methods to study the structure and dynamics of enveloped viruses.

II. MATERIALS AND METHODS

A. Macro-scale cultivation and purification of Sindbis virus

Protocols for growth and purification of Sindbis virus were followed as previously reported (Hernandez and Brown, 2005), with modifications for large-scale production.

Baby hamster kidney cells (BHK) were cultivated by passage in minimal essential medium (MEM) supplemented with 5% fetal bovine serum (FBS), 5% tryptose phosphate broth, 2 mM L-glutamine, and 50 μg/ml gentamicin. Cells were grown to near confluence in 875 cm^2 multi-level flasks (Falcon) prior to infection with a heat-resistant strain of the Sindbis virus (SVHR) at a multiplicity of infection (MOI) of 0.02 (0.02 virus particles/cell). Cells were refed with Glasgow MEM (GMEM) containing the same supplements plus an additional 2 g/l of $NaHCO_3$, following infection. Virus particles were harvested from the growth medium at 25 h post-infection.

Virus particles were purified by centrifugation through gradients of potassium tartrate (dibasic hemihydrate) in PN Buffer (50 mM PIPES pH 7.2, 100 mM NaCl). Growth media containing extracellular virus particles were clarified by slow speed centrifugation prior to being loaded onto continuous 15%–37% (w/v) potassium tartrate density gradients. Gradients were run at 100 000× g for 4 h (Fig. 1). Gradients were fractionated. Fractions containing the virus were combined and applied to a step gradient of 37% and 15% potassium tartrate. The virus particles were collected from the fractions at the interface between the 15% top and 37% bottom layer of potassium tartrate. Fractions were subsequently dialyzed against PN buffer to remove the potassium tartrate. The virus particles were then sedimented by ultracentrifugation at 100 000× g for 2 h. The resulting virus pellets were resuspended in PN buffer and the concentration was adjusted to either 1 mg/ml or 4 mg/ml. The concentration was determined by using the Lowry Assay method for the estimation of membrane protein concentrations (Markwell *et al.*, 1978).

Sample purity was determined by denaturing sodium dodecyl sulfate polyacrylamide gel electrophoresis (SDS-PAGE) (Fig. 2, lane 2). The tricine-SDS-PAGE protocol established by Schägger (2006) was used. Gels were silver stained using a commercial kit (Pierce). Purified virus particles were imaged by transmission electron microscopy (TEM) on copper grids after staining with 2% uranyl acetate for 30 s.

B. Micro-crystallization

The production of Sindbis virus macrocrystals in vapor diffusion drops was previously described by Harrison *et al.* (1992). This method was adapted to produce showers of microcrystals. The precipitant solution was 5.5% w/v PEG 8000, 7.5% w/v glycerol, and 240 mM KCl. A total of 195 hanging drops were prepared by mixing 5 μl of the 1 mg/ml concentration of purified Sindbis virus in PN buffer with 5 μl of the precipitant solution in each drop. An additional 30 hanging drops were likewise prepared using the 4 mg/ml Sindbis sample. Hanging drops were allowed to equilibrate with 500 μl of the precipitant solution by vapor diffusion for at least 4–5 days at 4 °C. EasyXtal (Qiagen) 15-well plates equipped with screw-in crystallization supports were used. The density of microcrystals was estimated by counting the number of crystals in a

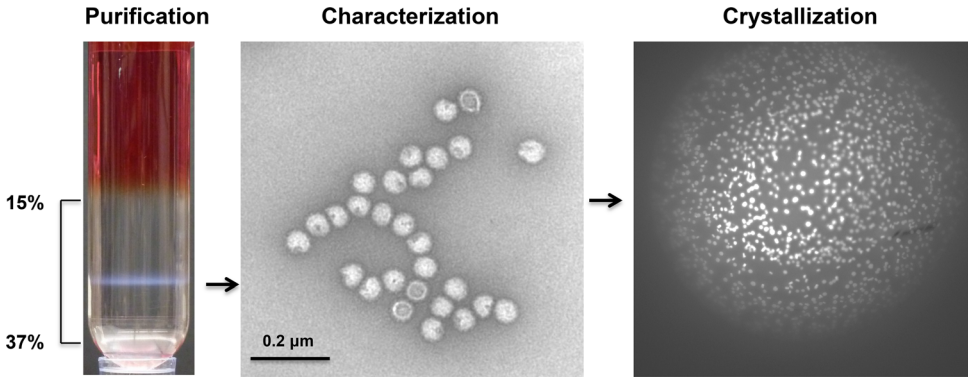

FIG. 1. Purification of Sindbis virus by centrifugation through a continuous potassium tartrate gradient, followed by characterization of the sample using transmission electron microscopy (TEM), and characterization of the crystals using UV fluorescence microscopy is illustrated. The TEM image of purified Sindbis virions is at 53 000× magnification.

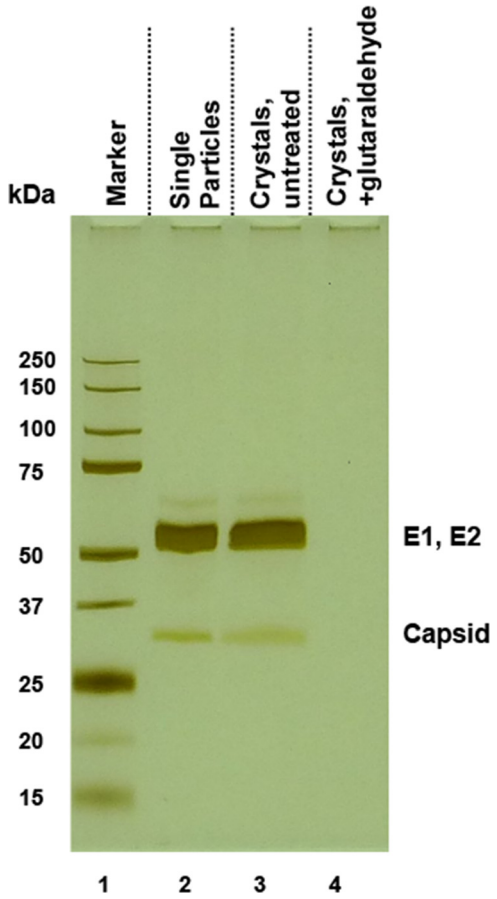

FIG. 2. SDS-PAGE analysis of microcrystals prepared from purified Sindbis virus. Untreated single particles are shown in lane 2. Untreated dissolved crystals are shown in lane 3. Crystals treated with an amount of glutaraldehyde comparable to the 0.5% used for the experiments are shown in lane 4. Proteins E1 and E2 are approximately the same molecular weight (47.5 kDa and 46.7 kDa, respectively) and are therefore not resolved on the gel. Glutaraldehyde treatment results in a complete crosslinking of the proteins in the virus particles, which results in the disappearance of individual protein bands on the gel.

small volume using a hemacytometer and an optical microscope. Crystallization with a 1 mg/ml and 4 mg/ml sample was expected to produce 25 μm and 50 μm crystals, respectively.

C. Virus inactivation

To meet biosafety requirements for SFX data collection at the Linac Coherent Light Source (LCLS), infectivity of Sindbis virus microcrystals was abolished by glutaraldehyde treatment. Once microcrystals had formed, glutaraldehyde was added to the precipitant volume in all crystallization plate reservoirs to a final concentration of 0.5% (v/v) and allowed to equilibrate with the volume in each crystal drop by vapor diffusion for 4–5 days at 4 °C. The volume of all crystal drops was then combined.

Inactivation of all microcrystals used for the experiments was confirmed by plaque assays. A sample of the glutaraldehyde treated microcrystals was diluted ten-fold in PN buffer supplemented with 3% FBS, and warmed at 37 °C for 1 h to dissolve the crystals. Ten-fold serial dilutions were prepared and assayed by duplicate plaque titration. Untreated microcrystals were likewise assayed in parallel as a control. After 48 h, cells were stained with 0.05% neutral red and plaques were counted. The limit of detection with this assay was 25 plaque forming units (pfu) per ml, a measure of infectious virus particles.

Glutaraldehyde is known to react with various amino acid functional groups to form covalent crosslinks within a protein or among proteins (Migneault *et al.*, 2004). Crosslinking of viral

proteins results in the particles being rendered non-infectious. SDS-PAGE of the glutaraldehyde treated crystals was used to confirm crosslinking and provide additional evidence of inactivation (Fig. 2, lanes 3–4).

D. Serial femtosecond X-ray crystallography

Sindbis virus microcrystals were mixed with an agarose-based viscous medium for delivery to the XFEL beam according to methods previously established with protein crystals (Conrad, 2015). The 25 μm Sindbis crystals were first concentrated by centrifugation at 4000× g for 3 min, followed by resuspension in 20 μl of the mother liquor (41 mM PIPES pH 7.2, 82 mM NaCl, 4.5% PEG 8000, 7.75% glycerol, and 0.2M KCl). The 50 μm crystals were likewise concentrated and resuspended in 13 μl of the mother liquor. The agarose medium was prepared by dissolving 0.14 g of ultra low-melt agarose (Sigma-Aldrich) in 1.4 ml of crystal buffer and 0.6 ml of glycerol and heating to 95 °C for approximately 30 min. For each sample, four parts of the agarose medium were mixed with one part resuspended crystals, such that approximately 10^4 micro crystals were embedded in the agarose/sample mixtures that were subsequently injected. Optical light microscopy and UV fluorescence microscopy were used to confirm that the crystals withstood the mixing process.

Sindbis crystals in the agarose-based viscous medium were delivered to the XFEL beam at the Coherent X-ray Imaging (CXI) beamline of the SLAC LCLS (Boutet and Williams, 2010). The high viscosity medium injector (Weierstall *et al.*, 2014), coupled with a 50 μm or 75 μm diameter nozzle capillary, was used to deliver the sample to the X-ray beam. The Cornell-SLAC Pixel Array Detector (CSPAD) was positioned at 582 mm from the sample/beam intersection point. The XFEL pulses were ∼47 fs in duration at 6 keV (2.066 Å), with approximately 6×10^{10} photons/pulse (120 Hz). The XFEL beam was focused to a diameter of ∼1.3 μm.

III. RESULTS AND DISCUSSION

A. Sample yield, purity, and crystallization

To produce a sufficient number of virus crystals, large-scale preparations of highly purified virus were necessary. Using the Lowry assay, we determined that ∼0.3 mg of purified Sindbis virus was produced from the infection of confluent BHK cell monolayers in each 875 cm^2 multi-level flask. 1 mg of Sindbis virus is roughly equivalent to 3×10^{11} pfu. Following purification by ultracentrifugation through potassium tartrate gradients, highly purified virus was obtained, and characterized by TEM (Fig. 1) and SDS-PAGE (Fig. 2, lane 2).

The density of microcrystals produced from the pooled vapor diffusion drops was $\sim 10^5$ crystals/ml. Crystals prepared from the 1 mg/ml concentration sample were up to 25 μm across a hexagonal face (sample A) (Fig. 3(a)), while at 4 mg/ml, crystals exhibited diameters up to 50 μm (sample B) (Fig. 3(b)). Crystal thickness was about 1/3 of the diameter. Crystals were neither birefringent nor detectable by second-order nonlinear optical imaging of chiral crystals (SONICC) (Kissick *et al.*, 2011) but did manifest strong UV absorbance (Fig. 1). The microcrystals were dissolved and analyzed by SDS-PAGE, where separation of the structural proteins E1 (47.5 kDa) and E2 (46.7 kDa) and the capsid protein (29.4 kDa) confirmed the presence of the expected proteins in the virus crystals (Fig. 2, lane 3).

B. Inactivation of virus infectivity

Treatment of microcrystals with glutaraldehyde was successful at eliminating infectivity of the Sindbis crystals. SDS-PAGE showed the disappearance of bands corresponding to the individual structural proteins in the treated sample, which is indicative of crosslinking (Fig. 2, lane 4). Complete inactivation was confirmed by the observation of no detectable infectious virus in plaque assays of the treated crystals. The parallel control plaque assay for virus infectivity in the untreated Sindbis crystals produced a titer of 2.5×10^8 pfu/ml.

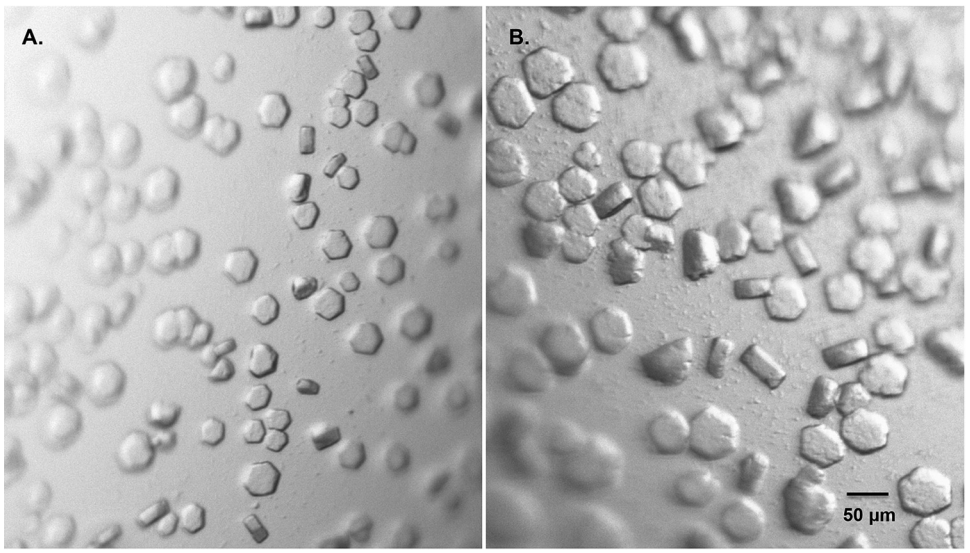

FIG. 3. Images of microcrystals prepared from virus at 1 mg/ml (a) and 4 mg/ml (b) of Sindbis virus prior to glutaraldehyde treatment. Samples A and B crystals exhibited sizes up to 25 μm and 50 μm, respectively. Scale bar = 50 μm.

C. XFEL diffraction

A total of 5685 diffraction patterns were identified as crystal hits from 709 196 events (0.8% average hit rate) during 98 min of sample injection. The hit rates from samples A (maximum diameter of 25 μm) and B (maximum diameter of 50 μm) were very similar. Hit finding and detector signal-calibration were carried out using Cheetah (Barty *et al.*, 2014). An event was considered a crystal hit if it contained over 15 isolated peaks with a signal-to-noise ratio of at least 6. Most of the patterns had fewer than 50 peaks (Fig. 4(a)). The majority of the diffraction patterns featured strong diffuse scattering between Bragg spots, which is discussed in Section III D. The resolution, sharpness of spots, and visibility of diffuse scattering varied significantly between patterns (Fig. 5). The diffuse scattering ranged from concentric hexagons (Fig. 5(a)) in single crystal patterns to isotropic concentric rings (Figs. 5(b)–5(d)) as the number of crystal mosaic blocks in the beam increased (indicating internal disorder). These diffuse rings resembled small angle X-ray scattering (SAXS) from a large spherical particle.

The crystal diffraction patterns were processed with the CrystFEL software suite (White *et al.*, 2013) using MOSFLM (Leslie and Powell, 2007) for indexing. A total of 562 patterns (10%) could be indexed with a rhombohedral unit cell, where $a = 652 \pm 27$ Å, $b = 664 \pm 30$ Å,

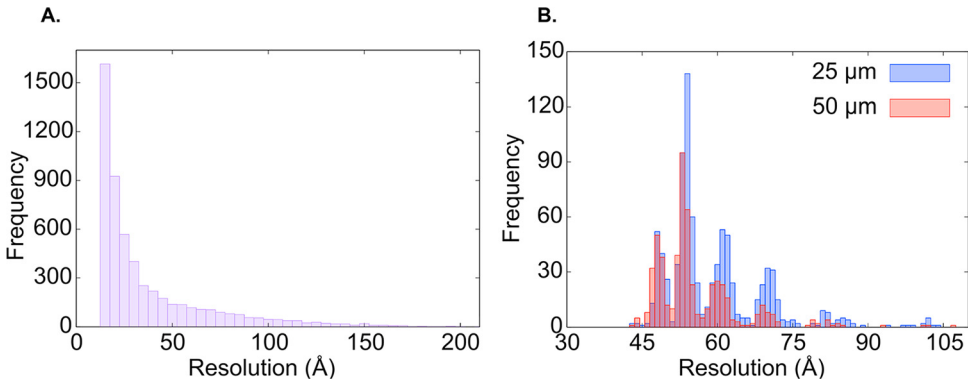

FIG. 4. (a) The number of Bragg peaks per diffraction pattern varied among collected patterns. The majority of the patterns collected had fewer than 50 peaks. (b) The distribution of resolution ranges in the 562 indexed diffraction patterns. Sample A (25 μm crystals) and sample B (50 μm crystals) were comparable in terms of resolution limits.

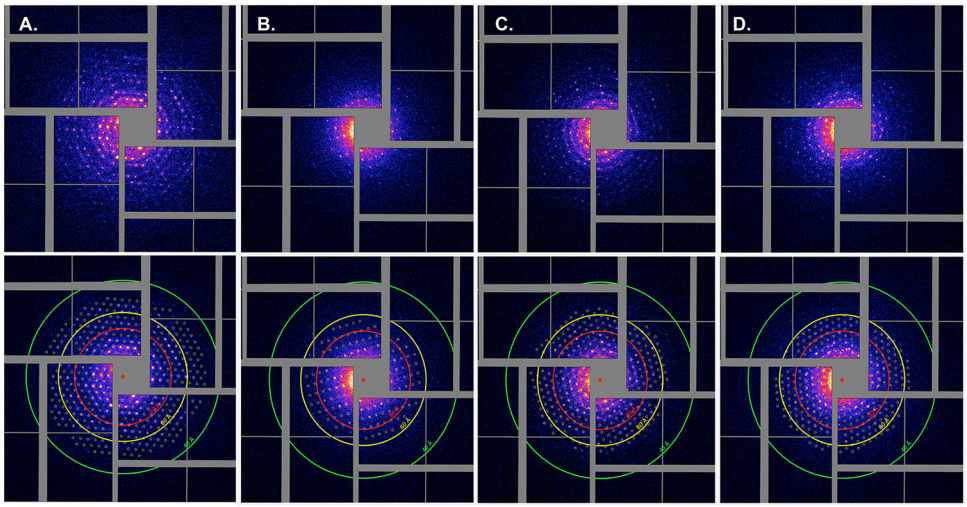

FIG. 5. Examples of X-ray diffraction patterns collected from Sindbis microcrystals at the LCLS CXI endstation are shown to illustrate variations in intensity and background scattering that were observed. Original images are shown (top panels) and predicted Bragg spots and resolution are indicated (bottom panels).

c = 662 ± 30 Å, $\alpha = 114.2 \pm 3.4°$, $\beta = 114.6 \pm 3.8°$, and $\gamma = 114.0 \pm 3.7°$, fitting a single Sindbis virus particle per unit cell. The unit cell distribution is shown in Fig. 6. Within this set, only 65 patterns could be indexed with a strictly rhombohedral cell, with a $\sim$ 670 Å, $\alpha \sim 115°$, and 6 patterns were indexed with a $\sim$785 Å and $\alpha \sim 115°$. Despite the high accuracy of predicted peak locations, the low resolution of these data does not permit us to determine whether the broad unit cell distribution is inherent to the crystals (potentially exacerbated by dehydration during sample delivery into vacuum), or a limitation of the indexing due to the small angular spread of observed reflections. The virtual powder pattern from the indexed patterns (Fig. 7) shows the broad rings indicative of a range of unit cell sizes.

The previously reported Sindbis crystal unit cell (Harrison *et al.*, 1992), where $a = b = 640$ Å and $c = 1520$ Å, was presumed to contain two Sindbis particles per (hexagonal) unit cell. The volume of their equivalent rhombohedral cell, where $a = 627$ and $\alpha = 61.4°$, is somewhat smaller than our cell, which may be due to the temperature and crystallization differences.

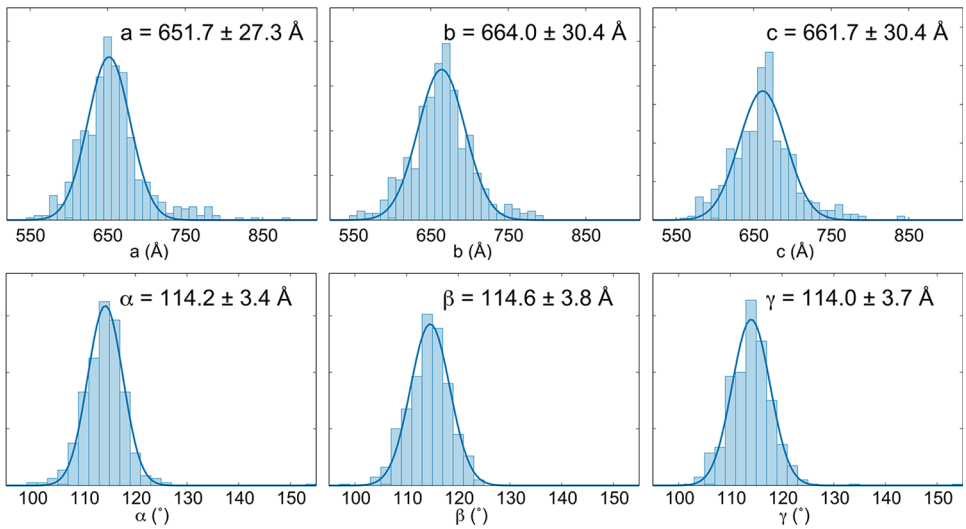

FIG. 6. Unit cell value distribution from combined indexing results of 562 patterns. Values indicate a rhombohedral space group, with one virus per unit cell.

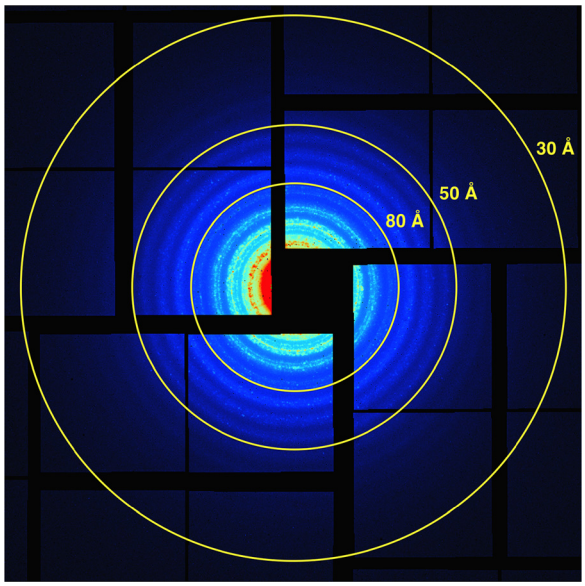

FIG. 7. Virtual powder diffraction pattern created from a composite of all indexed patterns with annotated resolution rings.

The resolution range of the indexed partial datasets is 287–43 Å, with no observable difference between resolution limits of samples A and B (Fig. 4(b)), despite the difference in crystal size. The histogram of the resolution limits slightly underestimates the highest resolution peaks in the patterns by 1–2 diffraction orders. This is a result of necessarily using a higher intensity threshold than the weakest diffraction spots during hit finding, in order to minimize the number of false positive hits.

During the extremely brief XFEL pulses (∼45 fs in this experiment), crystals do not have time to rotate and, together with the narrow SASE (self-amplified spontaneous emission) bandwidth (0.1%) and low divergence, this leads to the collection of still diffraction patterns. As a result, almost all observed reflections are partials, requiring high multiplicity (number of times a symmetry related reflection is sampled) to accurately determine the structure factors. Crystals with a high degree of disorder, such as the Sindbis virus crystals, require an even higher multiplicity to be able to average out over the heterogeneities. A significantly larger dataset, which extends to higher resolution, will be necessary to confirm the space group.

D. Analysis of XFEL small angle diffuse scattering

To gain some insight into the observed diffuse scattering, we analyzed the data in the context of small angle scattering. Signal to noise ratio was improved by combining the signal from all 5685 hits and calculating the median intensity for each pixel across all patterns. Combining the diffuse scattering intensities from the 5685 randomly orientated diffraction patterns resulted in a single isotropic pattern (Fig. 8). To improve the signal-to-noise ratio, each pixel was assigned a radial distance from the center of the image, and the average of intensity at each radial bin was calculated to yield a final intensity profile as a function of q, while masking out the gaps between modules in the detector. The background contributed by solvent scattering was determined from images not categorized as hits and subsequently subtracted from the signal. The intensity profile generated from images not categorized as hits did not exhibit a SAXS-like pattern (Fig. 9). This indicates that the observed scattering does not arise from SAXS of free virus particles suspended in the delivery medium but is associated with the microcrystals.

The XFEL experimental setup is designed for high to medium resolution X-ray diffraction studies, rather than very low-resolution data typically collected in SAXS experiments. The resolution necessary to reliably determine size and shape of a particle from SAXS is twice the

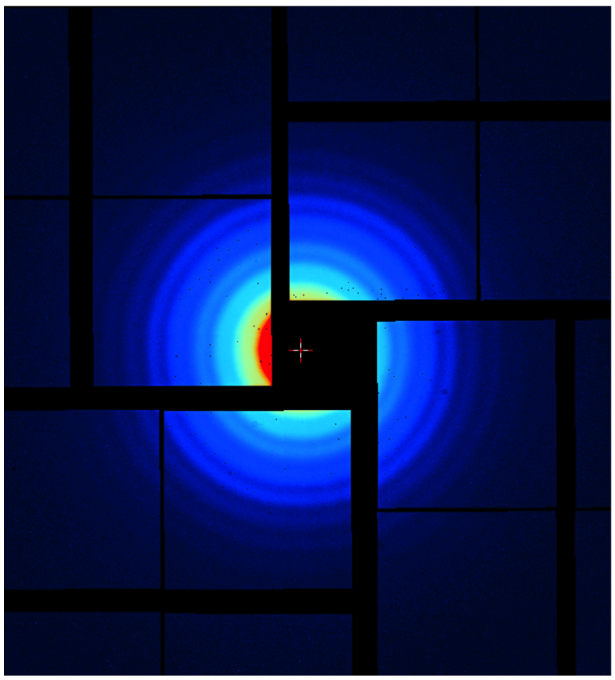

FIG. 8. Combination of the diffuse patterns from the 5685 randomly orientated diffraction patterns results in a single isotropic pattern.

maximum dimension of the particle. The estimated dimension of Sindbis, based on SANS studies, is 676–720 Å (He *et al.*, 2012). True SAXS analysis requires data with resolution lower than 1360–1440 Å—well below the minimal 363 Å resolution that we were able to collect with the maximal possible detector distance.

To assess whether the diffuse rings may be attributed to SAXS from Sindbis virus particles, we calculated a SAXS profile from the low-resolution electron density map from a cryoEM

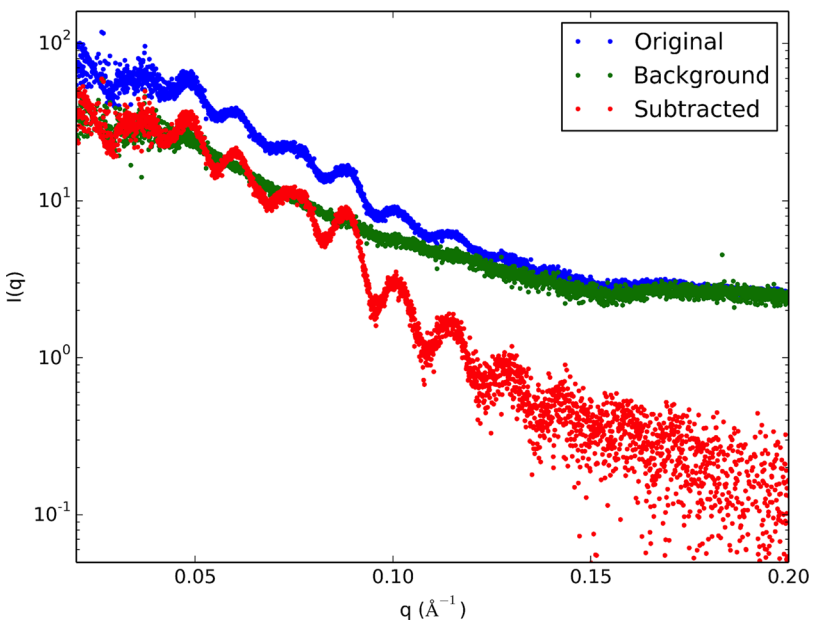

FIG. 9. The intensity profile generated from the combined median values shown in Fig. 7, with and without the calculated background intensity subtracted.

model of Sindbis at pH 6.4 (Cao and Zhang, 2013), taking into account the varying densities present in the particle. The electron density map was converted to a volumetric model of 15 Å diameter beads, and the electron density was stored in the B-factor column of the resulting PDB file (Wriggers, 2010). The Debye equation was then used to calculate the SAXS profile, which yielded a radius of gyration (R_g) of 247.3 Å and D_{max} of 680 Å. The spacing between the maxima of the concentric rings of this simulated profile, which is directly related to particle size (Glatter and Kratky, 1982), was 0.0130 $Å^{-1}$. This is consistent with what was observed in the experimental profile from Sindbis microcrystals, which was 0.0132 $Å^{-1}$, suggesting that the diffuse scatter seen in the XFEL data arises from the small angle scattering of Sindbis virus particles. However, direct comparison of the simulated profile and the experimental profile does reveal discrepancies in features such as peak height, and slight variations in spacing between individual peaks (Fig. 10). These differences may result from assuming a solution of monodisperse, non-interacting virus particles when calculating the SAXS profile using the Debye equation. However, in this experiment, the diffuse scattering arises not from particles floating freely in solution but from particles packed tightly in a crystal. Significant inter-particle interactions occur as demonstrated by the bright Bragg spots. These inter-particle interactions may manifest as other forms of diffuse scattering, which might also explain the differences between the simulated and experimental SAXS patterns. Nonetheless, the agreement between the average spacing of concentric rings of the diffuse scattering and the simulated SAXS pattern of the virus particle suggests that the non-Bragg scattering is a consequence of underlying molecular transforms of the individual particles.

Diffuse scattering from virus crystals was also observed in 25 Å diffraction patterns from enveloped virus West Nile virus crystals (Kaufmann *et al.*, 2010). Partially disordered crystals of the internal lipid membrane-containing bacteriophage PRD1 also produced diffuse rings that overlayed with Bragg peaks, and the radial ring separation was consistent with solution scattering (Bamford *et al.*, 2002). This indicates that size of the bacteriophage in the crystals is similar to the solution state. As noted earlier, the presence of lipid makes crystals of enveloped viruses particularly prone to disorder, and any departure from translational symmetry will produce diffuse scattering between the Bragg reflections (Rossmann, 2013). However, X-ray diffraction of crystals of the non-enveloped HK97 bacteriophage head also showed similar rings among the lower-resolution Bragg peaks (Tsuruta *et al.*, 1998). This suggests that the background

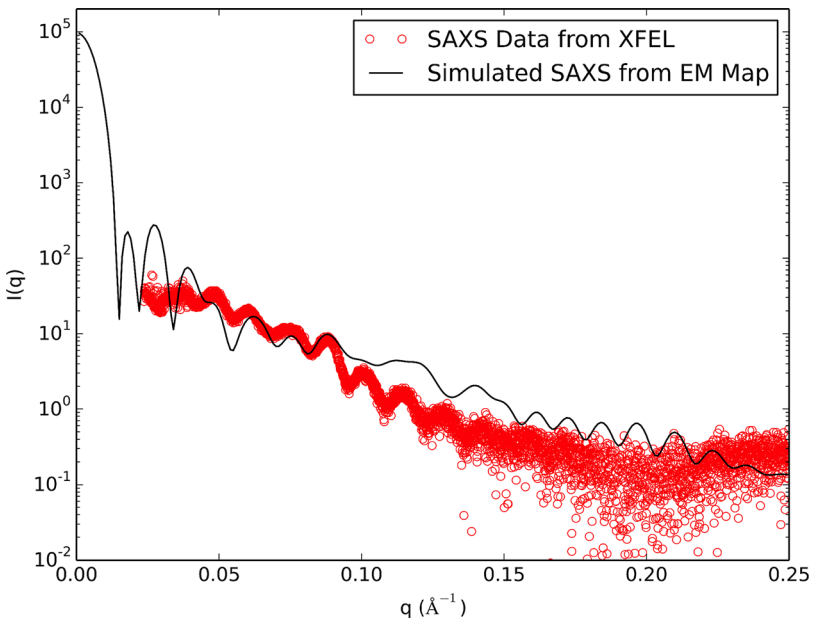

FIG. 10. The simulated SAXS profile of Sindbis generated from an EM electron density map, compared to the experimental SAXS profile generated from XFEL crystal diffraction data.

scattering could also be caused by other factors, such as heterogeneity in the sample due to ordering of a second phase, rather than an average over many defects, which would produce isotropic scattering. Even if the particles are structurally identical in terms of protein arrangement, an important consideration is the organization of RNA or DNA genome in a capsid, which may differ among the particles (Fry *et al.*, 1999). The fact that the diffuse scattering from individual shots is not entirely isotropic suggests that the genomes may occur in a limited set of orientations, rather than a continuous distribution. Simulations of the diffuse scattering based on models may be used to determine the possible registration of the genome relative to the capsid. Single-stranded RNA genomes, like that of Sindbis, are assembled through interactions between the genome and capsid or nucleocapsid proteins in the confines of the capsid or virus particle, and some do organize in line with their symmetry (Speir and Johnson, 2012).

E. Summary and Conclusions

Serial crystallography with a femtosecond pulsed XFEL has been established in recent years as a viable approach for investigating protein crystal structures (Chapman *et al.*, 2011). Here, we report the first attempts to extend the technique to virus crystallography. Our results provide a foundation of experience that future virus XFEL crystallography and solution scattering experiments can build upon. Although this effort did not produce diffraction at a higher resolution than previously reported, in spite of the high flux XFEL beam, the data provide evidence for a rhombohedral space group for enveloped Sindbis virus crystals. It is apparent that resolution is limited by the inherent nature of the sample, rather than the quality of the X-rays.

Delivery of the virus crystals to the beam in the viscous agarose medium proved to be a significant technical improvement. Agarose enables more efficient delivery of sample to the beam, thus reducing the amount of sample needed for measurement (Conrad *et al.*, 2015). The agarose medium produced minimal background scattering, particularly in the low to mid-resolution range where diffraction was measured for the Sindbis crystals.

One of the most interesting results reported here is the simultaneous appearance of diffuse scattering and Bragg peaks produced from crystals. Our analysis indicates that the SAXS-like diffuse scattering originates from the crystals, not from free virus particles in solution. Information from the scatter produces a SAXS-like profile that is similar to a calculated profile from a model of Sindbis that was derived from cryoEM of virus particles. The extent to which factors that were discussed above contribute to the diffuse scattering will require further investigation. An improved understanding of this phenomenon will lead to an appreciation of how useful this data may be in providing additional structural information about the ordering of virus particles and their genomes in a crystal lattice.

ACKNOWLEDGMENTS

This work was funded by the U.S. National Science Foundation (NSF) Award No. 1120997, NSF STC BioXFEL center Award No. 1231306, and National Institutes of Health (NIH) Grant Nos. GM097463-04, GM108635, and 1R01GM095583, and the PSI:Biology Center MPID U54GM094625. Part of this research was carried out at the LCLS, a National User Facility operated by Stanford University on behalf of the U.S. Department of Energy, Office of Basic Energy Sciences. We thank Dr. Raquel Hernandez at North Carolina State University for providing the initial stock of Sindbis virus and advice on growth and purification. We thank David Lowry in the Arizona State University CLAS Bioimaging Facility Electron Microscopy Lab for technical assistance in operation of the transmission electron microscope. We also thank Dr. Edward Snell and Dr. Eaton Lattman at Hauptman-Woodward Medical Research Institute for helpful discussions and suggestions.

Abrescia, N. G. A., Cockburn, J. J. B., Grimes, J. M., Sutton, G. C., Diprose, J. M., Butcher, S. J. *et al.*, "Insights into assembly from structural analysis of bacteriophage PRD1," Nature **432**, 68–74 (2004).
Abrescia, N. G. A., Grimes, J. M., Kivelä, H. M., Assenberg, R., Sutton, G. C., Butcher, S. J. *et al.*, "Insights into virus evolution and membrane biogenesis from the structure of the marine lipid-containing bacteriophage PM2," Mol. Cell **31**, 749–761 (2008).

Aquila, A., Hunter, M. S., Doak, R. B., Kirian, R. A., Fromme, P., White, T. A. *et al.*, "Time-resolved protein nanocrystallography using an X-ray free-electron laser," Opt. Express **20**, 2706 (2012).
Bamford, J. K. H., Cockburn, J. J. B., Diprose, J., Grimes, J. M., Sutton, G., Stuart, D. I. *et al.*, "Diffraction quality crystals of PRD1, a 66-MDa dsDNA virus with an internal membrane," J. Struct. Biol. **139**, 103–112 (2002).
Barty, A., Caleman, C., Aquila, A., Timneanu, N., Lomb, L., White, T. A. *et al.*, "Self-terminating diffraction gates femtosecond X-ray nanocrystallography measurements," Nat. Photonics **6**, 35–40 (2011).
Barty, A., Kirian, R. A., Maia, F. R., Hantke, M., Yoon, C. H., White, T. A., and Chapman, H., "Cheetah: Software for high-throughput reduction and analysis of serial femtosecond X-ray diffraction," J. Appl. Crystallogr. **47**, 1118–1131 (2014).
Boutet, S. and Williams, G. J. "The Coherent X-Ray Imaging (CXI) instrument at the Linac Coherent Light Source (LCLS)," New J. Phys. **12**, 035024 (2010).
Cao, S. and Zhang, W. "Characterization of an early-stage fusion intermediate of Sindbis virus using cryoelectron microscopy," Proc. Natl. Acad. Sci. U. S. A. **110**, 13362–13367 (2013).
Carstens, E. B., *Part I: Introduction, Ninth Report of the International Committee on Taxonomy of Viruses* (Elsevier, Inc., 2012).
Chapman, H. N., Caleman, C., and Timneanu, N., "Diffraction before destruction," Philos. Trans. R. Soc., B **369**, 20130313 (2014).
Chapman, H. N., Fromme, P., Barty, A., White, T. A., Kirian, R. A., Aquila, A. *et al.*, "Femtosecond X-ray protein nanocrystallography," Nature **470**, 73–77 (2011).
Connolly, S. A., Jackson, J. O., Jardetzky, T. S., and Longnecker, R., "Fusing structure and function: A structural view of the herpesvirus entry machinery," Nat. Rev. Microbiol. **9**, 369–381 (2011).
Conrad, C. E., "A novel inert crystal delivery medium for serial femtosecond crystallography," IUCrJ **2**, 421–430 (2015).
Ekeberg, T., Svenda, M., Abergel, C., Maia, F. R. N. C., Seltzer, V., Claverie, J. *et al.*, "Three-dimensional reconstruction of the giant mimivirus particle with an X-ray free-electron laser," Phys. Rev. Lett. **114**, 098102 (2015).
Fenalti, G., Zatsepin, N. A., Betti, C., Giguere, P., Han, G. W., Ishchenko, A. *et al.*, "Structural basis for bifunctional peptide recognition at human δ-opioid receptor," Nat. Struct. Mol. Biol. **22**, 265 (2015).
Fry, E. E., Grimes, J., and Stuart, D. I., "Virus crystallography," Mol. Biotechnol. **12**, 13–23 (1999).
Fuller, S. D., "The T = 4 envelope of Sindbis virus is organized by interactions with a complementary T = 3 capsid," Cell **48**, 923–934 (1987).
Glatter, O. and Kratky, O., *Small Angle X-Ray Scattering* (Academic Press, London, 1982).
Grigorieff, N. and Harrison, S. C., "Near-atomic resolution reconstructions of icosahedral viruses from electron cryo-microscopy," Curr. Opin. Struct. Biol. **21**, 265–273 (2011).
Harrison, J. S., Higgins, C. D., O'Meara, M. J., Koellhoffer, J. F., Kuhlman, B. A., and Lai, J. R., "Role of electrostatic repulsion in controlling pH-dependent conformational changes of viral fusion proteins," Structure **21**, 1085–1096 (2013).
Harrison, S. C., Strong, R. I. L., Schlesinger, S., Schlesinger, M. J., Euclid, S., and Louis, S., "Crystallization of Sindbis virus and its nucleocapsid," J. Mol. Biol. **226**, 277–280 (1992).
He, L., Piper, A., Meilleur, F., Hernandez, R., Heller, W. T., and Brown, D. T., "Conformational changes in Sindbis virus induced by decreased pH are revealed by small-angle neutron scattering," J. Virol. **86**, 1982–1987 (2012).
Hernandez, R. and Brown, D., "Sindbis virus: Propagation, quantification, and storage," Curr. Protoc. Microbiol. **15B**, 1–34 (2005).
Holton, J. M. and Frankel, K. A., "The minimum crystal size needed for a complete diffraction data set," Acta Crystallogr., Sect. D: Biol. Crystallogr. **66**, 393–408 (2010).
Kaufmann, B., Plevka, P., Kuhn, R. J., and Rossmann, M. G., "Crystallization and preliminary X-ray diffraction analysis of West Nile virus," Acta Crystallogr., Sect. F: Struct. Biol. Cryst. Commun. **66**, 558–562 (2010).
Kissick, D., Wanapun, D., and Simpson, G., "Second-order nonlinear optical imaging of chiral crystals," Annu. Rev. Anal. Chem. **4**, 419–437 (2011).
Kupitz, C., Basu, S., Grotjohann, I., Fromme, R., Zatsepin, N. A., Rendek, K. N. *et al.*, "Serial time-resolved crystallography of photosystem II using a femtosecond X-ray laser," Nature **513**, 261–265 (2014).
Leslie, A. G. W. and Powell, H. R., "Processing diffraction data with mosflm," Evol. Methods Macromol. Crystallogr. **245**, 41–51 (2007).
Liu, W., Wacker, D., Gati, C., Han, G. W., James, D., Wang, D. *et al.*, "Serial femtosecond crystallography of G protein – Coupled receptors," Science **342**, 1521–1525 (2013).
Lundstrom, J. O. and Pfeffer, M., "Phylogeographic structure and evolutionary history of Sindbis virus," Vector-Borne Zoonotic Dis. **10**, 889–907 (2010).
Markwell, M. A., Haas, S. M., Bieber, L. L., and Tolbert, N. E., "A modification of the Lowry procedure to simplify protein determination in membrane and lipoprotein samples," Anal. Biochem. **87**, 206–210 (1978).
Migneault, I., Dartiguenave, C., Bertrand, M. J., and Waldron, K. C., "Glutaraldehyde: Behavior in aqueous solution, reaction with proteins, and application to enzyme crosslinking," Biotechniques **37**, 790–802 (2004).
Neutze, R., "Opportunities and challenges for time-resolved studies of protein structural dynamics at X-ray free-electron lasers," Philos. Trans. R. Soc., B **369**, 20130318 (2014).
Perera, R., Khaliq, M., and Kuhn, J., "Closing the door on flaviviruses: Entry as a target for antiviral drug design," Antiviral Res. **80**, 11–22 (2008).
Rossmann, M. G., "Synchrotron radiation as a tool for investigating virus structures," J. Synchrotron Radiat. **6**, 816–821 (1999).
Rossmann, M. G., "Structure of viruses: A short history," Q. Rev. Biophys. **46**, 133–180 (2013).
Schägger, H., "Tricine-SDS-PAGE," Nat. Protoc. **1**, 16–22 (2006).
Seibert, M. M., Ekeberg, T., Maia, F. R. N. C., Svenda, M., Andreasson, J., Jonsson, O. *et al.*, "Single mimivirus particles intercepted and imaged with an X-ray laser," Nature **470**, 78–82 (2011).
Song, C., Jiang, H., Mancuso, A., Amirbekian, B., Peng, L., Sun, R. *et al.*, "Quantitative imaging of single, unstained viruses with coherent X rays," Phys. Rev. Lett. **101**, 1–4 (2008).

Speir, J. A. and Johnson, J. E., "Nucleic acid packaging in viruses," Curr. Opin. Struct. Biol. **22**, 65–71 (2012).
Spence, J., "Approaches to time-resolved diffraction using and XFEL," Faraday Discuss. **171**, 429–438 (2014).
Tang, J., Jose, J., Chipman, P., Zhang, W., Kuhn, R. J., and Baker, T. S., "Molecular links between the E2 envelope glycoprotein and nucleocapsid core in Sindbis virus," J. Mol. Biol. **414**, 442–459 (2011).
Tenboer, J., Basu, S., Zatsepin, N., Pande, K., Milathianaki, D., Frank, M. *et al*., "Time-resolved serial crystallography captures high-resolution intermediates of photoactive yellow protein," Science **346**, 1242–1246 (2014).
Tsuruta, H., Reddy, V. S., Wikoff, W. R., and Johnson, J. E., "Imaging RNA and dynamic protein segments with low-resolution virus crystallography: experimental design, data processing and implications of electron density maps," J. Mol. Biol. **284**, 1439–1452 (1998).
Wang, D., Weierstall, U., Pollack, L., and Spence, J. C. H., "Liquid mixing jet for XFEL study of chemical kinetics," J. Synchrotron Radiat. **21**, 1364–1366 (2014).
Weierstall, U., "Liquid sample delivery techniques for serial femtosecond crystallography," Philos. Trans. R. Soc., B **369**, 20130337 (2014).
Weierstall, U., James, D., Wang, C., White, T. A., Wang, D., Liu, W. *et al*., "Lipidic cubic phase injector facilitates membrane protein serial femtosecond crystallography," Nat. Commun. **5**, 3309 (2014).
White, T. A., Barty, A., Stellato, F., Holton, J. M., Kirian, R. A., Zatsepin, N. A., and Chapman, H. N., "Crystallographic data processing for free-electron laser sources," Acta Crystallogr. D. Biol. Crystallogr. **69**, 1231–1240 (2013).
Wiley, D. C. and von Bonsdorff, C. H., "Three-dimensional crystals of the lipid-enveloped Semliki Forest virus," J. Mol. Biol. **120**, 375–379 (1978).
Wriggers, W., "Using Situs for the integration of multi-resolution structures," Biophys. Rev. **2**, 21–27 (2010).
Zhang, X., Ge, P., Yu, X., Brannan, J. M., Bi, G., Zhang, Q. *et al*., "Cryo-EM structure of the mature dengue virus at 3.5-Å resolution," Nat. Struct. Mol. Biol. **20**, 105–110 (2013a).
Zhang, W., Kaufmann, B., Chipman, P. R., Kuhn, R. J., and Rossmann, M. G., "Membrane curvature in Flaviviruses," J. Struct. Biol. **183**, 86–94 (2013b).
Zhang, W., Mukhopadhyay, S., Pletnev, S. V, Baker, T. S., Kuhn, R. J., Michael, G. *et al*., "Placement of the structural proteins in Sindbis virus placement of the structural proteins in Sindbis virus," J. Virol. **76**, 11645–11658 (2002).
Zhang, H., Unal, H., Gati, C., Han, G. W., Liu, W., Zatsepin, N. A. *et al*., "Structure of the Angiotensin receptor revealed by serial femtosecond crystallography," Cell **161**, 833–844 (2015).
Zocher, G., Mistry, N., Frank, M., Hähnlein-Schick, I., Ekström, J.-O., Arnberg, N. *et al*., "A sialic acid binding site in a human Picornavirus," PLoS Pathog. **10**, e1004401 (2014).